JOURNAL OF Materials CHEMISTRY

Templated growth of calcite, vaterite and aragonite crystals on self-assembled monolayers of substituted alkylthiols on gold

Jörg Küther,[a] Ram Seshadri,[a] Wolfgang Knoll[b] and Wolfgang Tremel[a]

[a]*Institut für Anorganische Chemie und Analytische Chemie, Johannes Gutenberg-Universität Mainz Becherweg 24, Mainz D55099 Germany*

[b]*Max-Planck-Institut für Polymerforschung, Ackermannweg 10, Mainz D55128 Germany*

Making use of extensive scanning electron microscopy and the Rietveld analysis of X-ray diffraction profiles, we have studied the morphology, crystal habits and phase compositions of crystals of calcium carbonate grown on modified organic surfaces by precipitation from solution. The studies have been aimed at modeling natural biomineralization processes of the ubiquitous mineral forms of $CaCO_3$, *viz*. calcite, vaterite and aragonite. The parameters that could be controlled and were indeed found to drastically influence the crystallization were the thiol chain length, the ω-substituent on the thiol and the temperature at which crystallization was carried out. As many as ten different thiol modified substrates, apart from glass and clean gold surfaces were used for the templating. Such a heuristic study offers considerable insight into the nature of templated crystallization and has implications for the understanding of biomineralization processes.

In the hierarchy of inorganic structural chemistry, possibly the least well understood level of organization is that which takes place at the most macroscopic scale, namely the manner in which the crystallites of some materials assemble into well defined, high-performance architectures. The reason for the lack of understanding could very simply be that structural criteria at all lower levels of organization are important at each level. The number of examples by which biological systems are seen to construct in a facile manner very complex inorganic assemblies are legion.[1,2] Organizations of calcium carbonate crystals in biological systems in the three polymorphs calcite, vaterite and aragonite are well known illustrations of the so-called biomineralization processes. These processes take place usually at an organic–inorganic interface, the organic portion providing the initial structural information for the inorganic part to nucleate on and grow outwards in the desired manner. In other words the organic matrix which is easily manipulated and controlled acts as a structural template.[3–5]

Attempts to model the biomineralization process have usually made use of the templating features of large organic molecules, either freely in solution or organized at an interfacial boundary (Langmuir monolayers) or fixed on solid substrates.[3–5] Organic molecules can be synthesized and arranged, with atomic-level precision, making them templates of choice. Additionally, important physical properties such as the polarity of the exposed organic surface can be modified by selecting different functional groups. The discovery that thiols of long chain organic molecules bind strongly and specifically to metal (usually mercury, silver or gold) surfaces forming ordered monolayers, the self-assembled monolayers (SAMs),[6] has yielded an interesting class of molecular assemblies that permit the production of highly specific interfaces spread over relatively large areas.[7] Indeed SAMs are also made on silicon surfaces by the specific binding of silyl functionalities, and these have been used in model biomineralization studies.[8]

Many calcium containing biominerals including carbonates, phosphates (especially apatites and fluorapatites) and oxalates are found in nature. Of these, $CaCO_3$ makes up an attractive model mineral for studies in the laboratory, combining simple chemistry with diverse polymorphism, each polymorph in turn displaying morphologies or crystal habits that might be controlled and modified. Thus the three forms of $CaCO_3$ are found for example in the exoskeletons of algae and the eye lens of triblobites in the calcite modification; in ascidian spicules, egg shells of gastropods and in some gravity receptors in the vaterite modification; and in the nacreous layer of mollusc shells, human brain stones, gallstones and fish otoliths as aragonite.[9] Extensive studies on the phase stabilization and habit modification of $CaCO_3$ crystals grown under Langmuir monolayers and in the presence of organic, biological and ionic additives have been reported,[9,10] as have calcite crystallization on alkylsilane coated Si (001) surfaces mentioned earlier.[8] Studies from the Weizmann Institute have focused on the effect of free and bound biological macromolecules (usually proteins) on $CaCO_3$ crystallization.[11–13]

This article presents the results of model biomineralization studies using clean and thiol modified gold surfaces as the templating substrate in an attempt to influence relative amounts and crystal habits of the three polymorphs of $CaCO_3$. The thiols are either short or long chain molecules, with and without ω-substituents. While the chain length controls the crystallinity of the substrate assembly, the ω-substituent is expected to affect slightly the spacings between the head groups and affect considerably the polarity of the substrate as seen by the ions as they arrive on the substrate. Crystallization has been carried out at two different temperatures, 22 ± 3 °C and 45 ± 2 °C. Our approach has been heuristic in the sense that the effect on $CaCO_3$ crystallization of surfaces modified by as many as ten different thiols has been followed, apart from the effect of clean glass and clean gold surfaces. Detailed atomic force microscopy (AFM) studies on the substrates and attempts to obtain the morphologies of the 'early' crystals are underway and will not be presented here. A communication on the preference for aragonite on polar surfaces when the crystallization is carried out at 45 ± 2 °C has been made.[14]

Experimental

Chemicals

$CaCl_2 \cdot 4H_2O$ (Suprapur), NaOH (PA), $(NH_4)_2CO_3$ (PA), H_2O_2 (medical, extra pure) hexadecanethiol (abbreviated C16H) (Synthesis grade), ethanol and methanol (PA) were purchased from Merck, ammonia (ACS) from Aldrich, and the sodium salt of mercaptopropanesulfonic acid (C3SO3Na) from Fluka. The last was recrystallised three times from methanol.

Undecanethiol (C11H) (98%) was bought from Lancaster. ω-Mercaptoundecanol (C11OH), the α,ω-dithiols of dodecane (C12SH) and hexadecane (C16SH), ω-mercaptoundecanoic acid (C11COOH), ω-mercaptohexadecanoic acid (C16COOH) and the sodium salt of ω-mercaptodecanesulfonic acid (C10SO3Na) were prepared and purified according to literature methods.[15] ω-Mercaptoundecanephosphonic acid (C11PO3H) was prepared by the reaction of $POCl_3$ with ω-mercaptoundecanol in anhydrous acetonitrile, following a procedure described by Putvinski *et al.*[16] Note that in our abbreviation scheme for the different thiols, the number in the abbreviation corresponds to the total number of carbon atoms in the chain.

Preparation of gold substrates and SAMs

Glass slides (B270/$38 \times 26 \times 1$ mm) were sonicated in propan-2-ol for 15 min, rinsed with water (Barnstead Easypure UV, $\rho > 18.3$ MΩ cm^{-1}) and further cleaned by use of a water–ammonia–H_2O_2 mixture (5 : 1 : 1, v/v/v), heating to 80 °C and holding for 10 min followed by rinsing with water and ethanol and then blowing dry with nitrogen gas. Evaporation of gold on to the glass substrates was done in an Balzer BAE 250 vacuum coating system at pressures lower than 5×10^{-6} hPa starting with a coating of 2 nm Cr to improve adhesion and then 48 nm Au (rate 0.05 nm s^{-1}). After 20 min of cooling in the evaporation chamber the slides were stored under Ar for not longer than 12 h before transferring to alcoholic thiol solutions of concentrations 1×10^{-4}–1×10^{-3} M. After 10–16 h in the adsorption solution they were removed, rinsed vigorously with ethanol to remove unbound thiols and blown dry with N_2. The SAMs were characterized by contact angle measurements and reflectance FTIR spectroscopy (not presented) and by surface plasmon resonance spectroscopy.

Growth experiments

Crystallization was performed in the manner shown in Fig. 1 Substrates were mounted by gluing on glass rods which were then fixed to the lid of the crystallization bath in a manner that held the active surface facing down. The crystallization bath contained 0.01 M $CaCl_2$ solution whose pH was adjusted to 10 using 0.1 M NaOH solution. The bath was then placed in a desiccator. For thermal equilibration the whole crystallization batch was placed in a digitally controlled oven (Heraeus Instruments). After *ca.* 1 h for equilibration, crystallization was started by placing a dish with 1.5 g of $(NH_4)_2CO_3$ at the bottom of the desiccator. The crystallization took place by the slow diffusion of CO_2 into the $CaCl_2$ bath over a 48 h period, following which the substrates were removed, rinsed with a small amount of water and blown dry with vigorous N_2 gas flow from a bottle. This last step is expected to remove $CaCO_3$ crystals which deposit adventitiously on the surface and are not tightly bound.

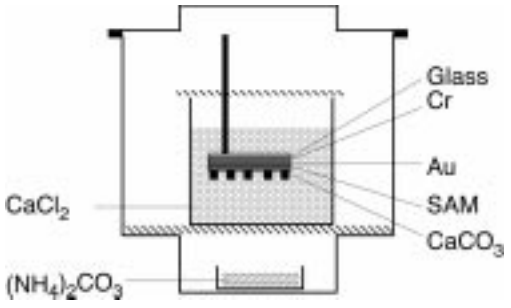

Fig. 1 Setup for the $CaCO_3$ crystallization experiments. This setup is placed in an oven whose temperature is controlled digitally.

X-Ray diffraction

The XRD experiments were performed in the $\theta/2\theta$ transmission geometry using a Siemens D5000 powder diffractometer with Ge(111) monochromatized Cu-Kα_1 radiation (1.540 56 Å). Crystals were scraped from the surface and mounted on Scotch™ tape. Data were collected from 20 to 60° 2θ, with a step size of 0.02° and a count time of 25 s per step. Because of the very small yields it was necessary to collect samples from three to four substrates for each experiment.

SEM studies

Microscopy was done with a Zeiss Digital Scanning Microscope 962 combined with an Kevex EDAX at acceleration potentials of 5–15 kV. The substrates on which the crystallizations were carried out were cut in small pieces and fastened with conducting glue on alumina sample holders and then sputtered with gold.

Surface plasmon spectroscopy (SPS)

SPS was used in the Kretschmann configuration to evaluate the thickness of the SAMs and in an attempt to follow kinetics of crystal growth. Sample slides were placed in a liquid filled Teflon cuvette. The backs of the slides were optically coupled to an LASFN9 prism ($n = 1.85$ at $\lambda = 632.8$ nm) using an optical matching fluid ($n = 1.70$). The optical source was a He–Ne laser ($\lambda = 632.8$ nm and maximum power 5 mW). The kinetic experiments were performed with a fixed beam, with the angle of incidence chosen such that the reflectivity was about 40% of the total.

Results

Crystallization kinetics and nucleation densities

Surface plasmon resonance spectroscopy (SPS) is an extremely sensitive technique, capable of detecting Å scale changes of the optical properties of a surface. Details of this technique can be found elsewhere.[17] To establish in a direct and simple manner that the substrate influences the crystallization of $CaCO_3$, we have performed a kinetic experiment on two very different thiol-modified gold surfaces; the thiols being the ω-mercaptohexadecanoic acid C16COOH and hexadecanethiol C16H. Both have the same carbon chain length of 16 and are expected to be well organised on the surface as evidenced from the SP spectra shown in Fig. 2 (a) and (b) for the two different surfaces. Simulations of the shift in the SP spectra using the Fresnel formula[18] suggest that both these surfaces are close packed monolayers and thus the structures of these two surfaces should be nearly identical. Their polarities are however quite different. The SP spectra allow one to chose an incident angle such that the tangent of the reflectivity is large, and hence is very sensitive to changes at the surface. This is seen to be at about 40% total reflectivity in the SP spectra. Monitoring the reflectivity as a function of time allows kinetics of changes on the surface to be followed in a relative manner. By filling the Teflon SPS cell with an aqueous 0.01 M $CaCl_2$ solution and running a tube from a sealed container of $(NH_4)_2CO_3$ into the cell, $CaCO_3$ precipitation is initiated on the surface which is followed by the SP reflectivity. Fig. 2(c) shows the time dependence of the SP reflectivity for $CaCO_3$ precipitation on the two surfaces mentioned. The measured signal is an average over the spot size of the laser beam, which is less than one millimeter in diameter. Crystallization on the polar surface of C16COOH is on average, clearly faster. Also, more material is deposited on this surface as seen from comparing the saturation reflectivities in the two cases.

Counting the density of crystals from SEM images after crystallization has occurred under similar conditions also yields the relative affinity of the surface of $CaCO_3$. Fig. 3 shows

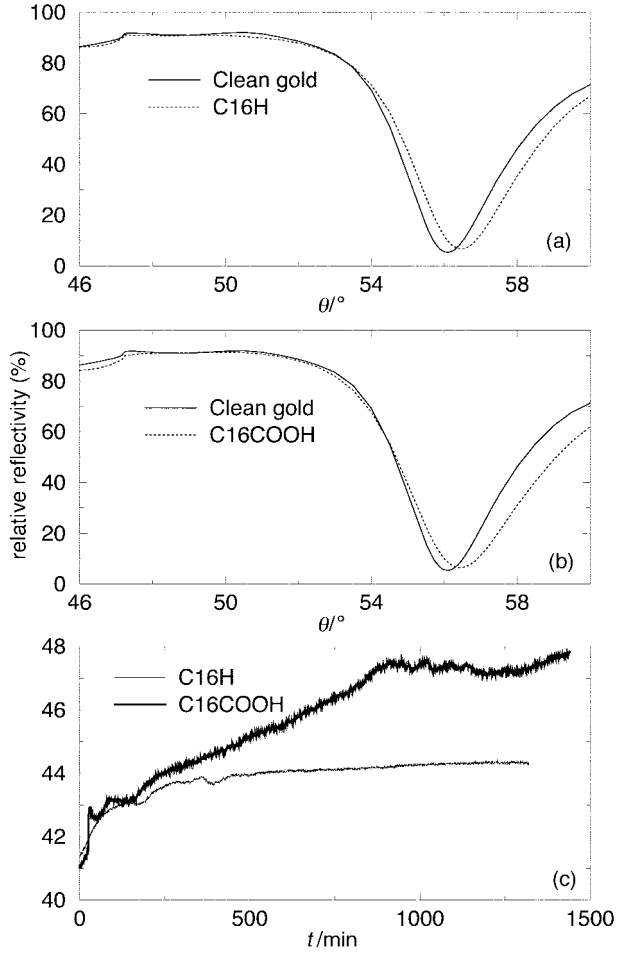

Fig. 2 (a) Surface plasmon spectra of clean and C16H covered gold surfaces. (b) Spectra of clean and C16COOH covered gold surfaces. (c) Time dependence of the surface plasmon reflectivity for the carboxylate terminated surface C16COOH and the alkyl terminated surface C16H monitoring the change on the surface as crystals are deposited. The slow diffusion of CO_2 into the cell commences at time $t=0$ min.

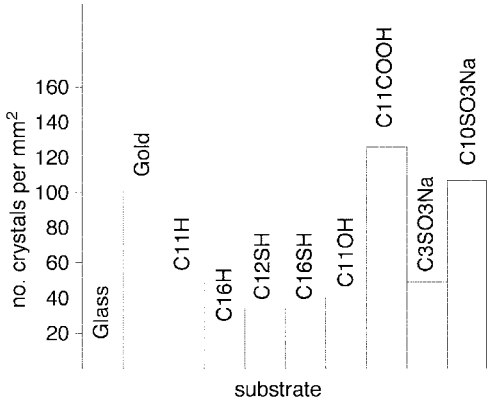

Fig. 3 Nucleation densities for $CaCO_3$ crystals on different substrates at 22 ± 3 °C

histograms of the nucleation densities on the different surfaces, averaged for each surface over many micrographs, for crystallizations carried out at 22 ± 3 °C. Clearly, the polar (C10SO3Na, C3SO3Na, C11COOH) surfaces are capable of nucleating a greater number of crystals than less polar surfaces. A surprising difference arises when the gold and glass surfaces are compared. The glass surfaces, being built up of relatively polar Si—O linkages are usually quite hydrophilic. However they are insulating so the initial ions from solution would tend to accumulate charges at the surface repelling other incoming ions of like polarity. Gold being a conductor, such charge build-up is not expected to take place, and this allows a greater nucleation density. The data for the glass surface are important since they serve as a reference; the crystals can either nucleate on the SAM surface or in solution, or on the glass walls of the chamber in which crystallization is carried out. The walls should be no more preferred as nucleation sites than the clean glass slides, and therefore nucleation densities greater than those obtained on glass (the preponderant case) suggest a preference for the SAM surface. Comparing the clean and derivatised gold surfaces, we see, as expected, that coating the high-energy gold surface with an inert (in terms of ω-functionality) long chain thiol such as C16H results in surfaces which are much poorer in inducing $CaCO_3$ crystallization.

Structures and modes of templating

As an overview of the analysis of compositions and morphologies of crystals of the different phases of $CaCO_3$ Fig. 4 shows SE micrographs of the typical habits of (a) calcite, (b) vaterite and (c) aragonite crystals, obtained from different surfaces. Fig. 5 shows simulations[19] of crystal habits for calcite, vaterite and aragonite emphasizing faces that are usually seen: structures were taken from the literature.[20–22] The key point in the discussion of templating effects is that the surface crystallinity is dictated by the Au(111) surface and almost all crystalline SAMs studied so far form a close packed hexagonal 2D lattice with a lattice parameter of *ca.* 5 Å.[23] SAMs formed by short alkyl chain thiols (usually with less than *ca.* 10 carbon atoms) do not order over long length scales however. Fig. 6, 7 and 8 show cuts along the actual crystal structures respectively of the three phases calcite, vaterite and aragonite, corresponding to the nucleating faces that give rise to the typical morphologies. For calcite (Fig. 6) the important nucleating plane observed in our crystals seems to be (001), which has the same symmetry and approximately the same interatomic spacings as crystalline thiol surfaces. In Fig. 6 for the (001) plane, the Ca and the carbonate groups are shifted from each other perpendicular to the representation. Sometimes, the crystals are seen to stand on edge signifying that the (110) plane is nucleated. The crystals are also occasionally seen to sit flat, which is the (104) plane, and this is the case when there is no templating. In the views of (110) and (104) all atoms are in the plane. Vaterite crystals are seen either sitting flat on (001) with the crystal and substrate sixfold axes in correspondence (Fig. 7) or on the (010) plane. The latter is surprising because a threefold axis cannot be easily identified. The aragonite crystal structure has no threefold symmetry, crystallizing in an orthorhombic space group. The crystals are usually seen to grow with a needle like morphology, with the needles often clustering. There are two kinds of oxygen atoms in this structure. The (001), (010) and the (100) projections of the aragonite structure are shown in Fig. 8.

Phase analysis from powder X-ray diffraction

The very distinct morphologies and rather disparate crystal sizes prevent quantification of amounts from the SAM surface by merely counting the number of crystals. Indeed, when more quantitative estimates by powder X-ray profile analysis are made as explained presently, we observe that even seemingly small numbers of calcite crystals in the SE micrographs actually correspond to quite large mass fractions, since the calcite crystals are always more compact and better crystallized than the vaterite and aragonite crystals. We have thus collected step-scanned X-ray powder profiles of the $CaCO_3$ crystals in the transmission geometry which allows reasonably good profiles to be obtained from the very small quantities involved, by transferring the crystals by scraping, from the SAM surface to Scotch™ tape. For each diffraction pattern, crystals had to be collected from three to four surfaces. The diffraction profiles

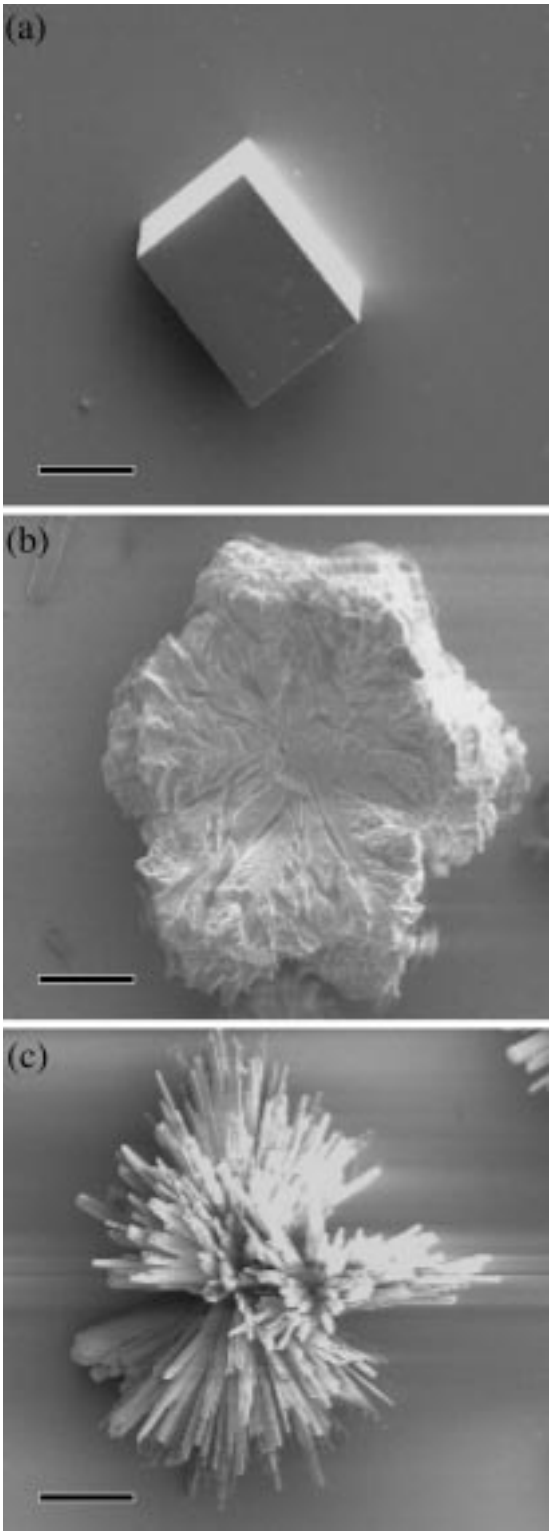

Fig. 4 SE micrographs of typical habits of the three $CaCO_3$ modifications as found on the surfaces discussed here: (a) calcite, (b) vaterite and (c) aragonite. The scale bar is 20 μm.

were then analyzed using the Rietveld method[24] incorporated in the XND program.[25] Lattice, profile and preferred orientation parameters were refined for each of the three phases, apart from the scale factors. Care was taken to scale the atom occupancies by the general Wyckoff multiplicity of the space group. Finally, the scale factors were inserted into the formula:[26]

$$W_j = \frac{(S_j Z_j M_j V_j / t_j)}{\Sigma_j (S_j Z_j M_j V_j / t_j)}$$

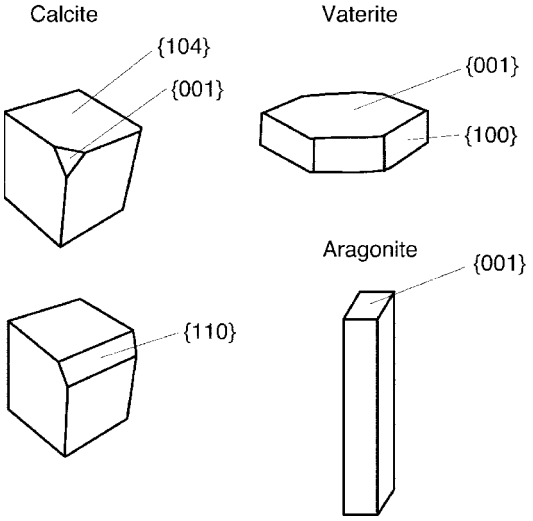

Fig. 5 Simulations of typical crystal habits of the phases of $CaCO_3$. The important faces are labelled.

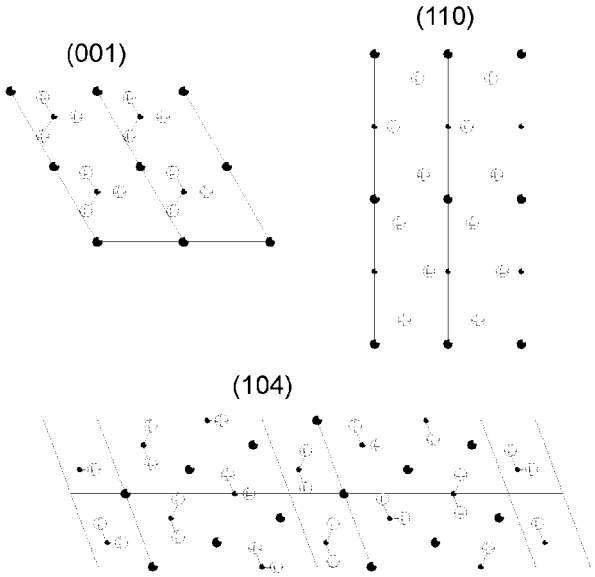

Fig. 6 Structure of calcite projected on the (001) (110) and (104) planes

where S_j = scale factor of phase j, Z_j = number of formula units of j per unit cell, M_j = mass per formula unit, V_j = unit cell volume and t_j = Brindley microabsorption factor,[27] in order to obtain the relative mass fractions W_j. The following assumptions have been made, which would affect the final accuracy of the estimate: (i) the X-ray sample is assumed to be a homogeneous powder, which is not correct because the small amounts of the crystals did not allow proper grinding. (ii) The Brindley[27] factors have been ignored since their calculation involves a knowledge of the average volumes of the crystallites in the powders and determining this in the present case is difficult because of the irregular morphologies. However, this last factor is unlikely to be important since the relative X-ray absorption coefficients are already small to start with and should not vary greatly across crystals with the same chemical formulation. The overall reliability of the estimates presented here is of the order of 5–10%. Importantly, the data seem to be consistent between experiments and in a relative manner, between analyses of the SE micrographs.

Fig. 9 shows typical X-ray diffraction patterns for $CaCO_3$ crystals obtained from a C10SO3Na surface (a) and from a C16COOH surface (b). These diffraction patterns are representative of calcite and vaterite rich surfaces, respectively. The refined contributions to the total profile from the individual

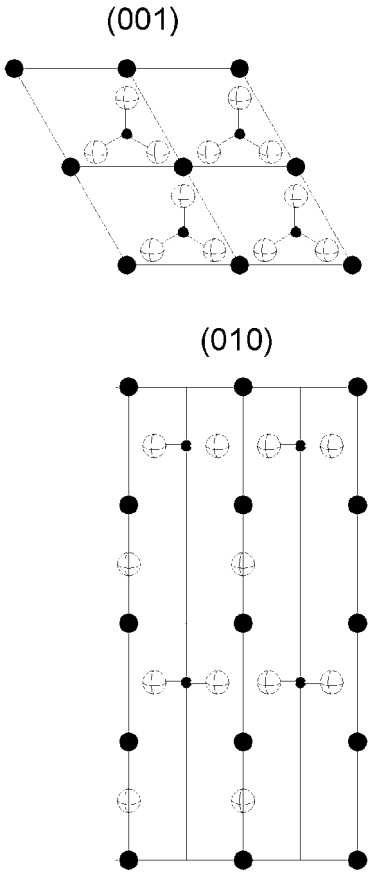

Fig. 7 Structure of vaterite projected on the (001) and (010) planes

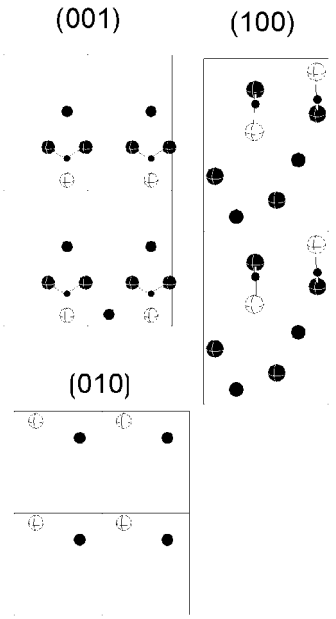

Fig. 8 Structure of aragonite projected on the (001), (100) and (010) planes. The two different oxygen atoms on the three coordinate C are represented as unfilled and filled, crossed spheres.

phases are shown below the experimental data as are the difference profiles (offset for clarity). In fitting such profiles, we find that the preferred orientation and linewidth parameters are quite revealing as to the nature of the crystals. The SE micrographs corresponding to these surfaces are shown in Fig. 10(a)–(d) at low and high magnifications. The acquisition and analysis of X-ray profiles of crystals grown on the different surfaces has allowed us to prepare a histogram of the phase compositions of samples collected after crystallization was

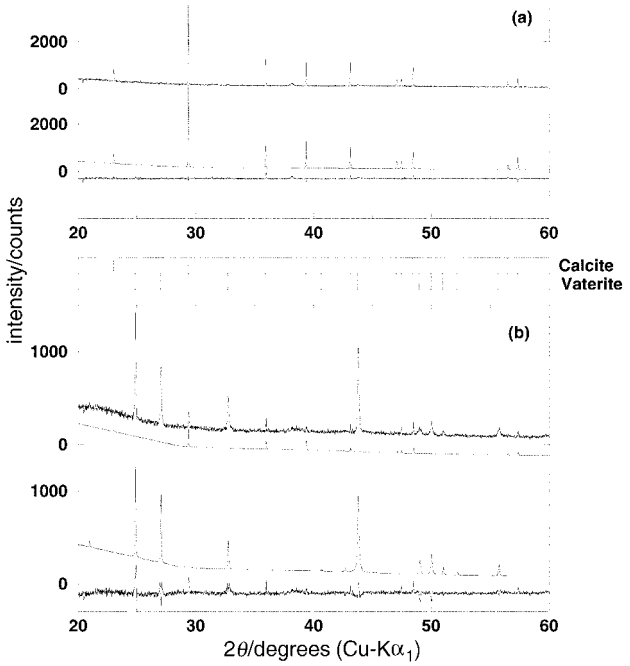

Fig. 9 Powder X-ray diffraction patterns of $CaCO_3$ crystals obtained from (a) C10SO3Na and (b) C16COOH surfaces at $22 \pm 3\,^{\circ}C$. X-Ray data, Rietveld fits for the calcite and vaterite contributions, and difference difference profiles are shown as are reflection position markers. The different traces have been offset for clarity.

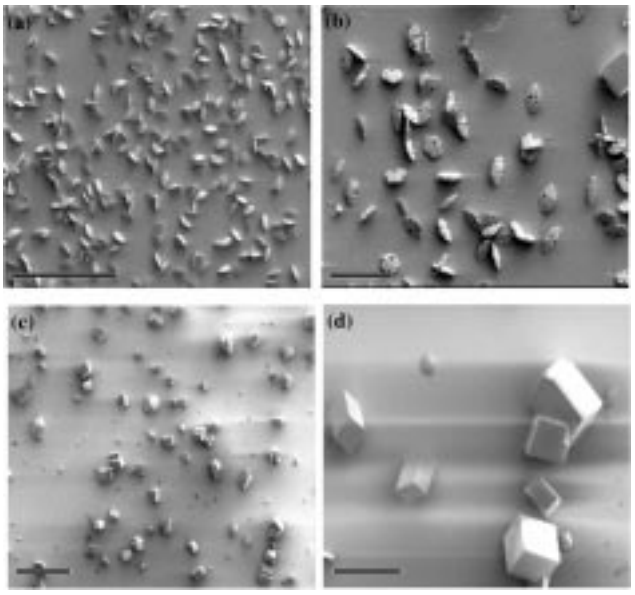

Fig. 10 SE micrographs of calcium carbonate crystals on C16COOH (a, b) and on C10SO3Na (c, d) modified gold surfaces at $22 \pm 3\,^{\circ}C$. (a, c) Low magnification (bars $\equiv$ 200 μm); (b, d) high magnification (bar $\equiv$ 50 μm).

carried out at $22 \pm 3\,^{\circ}C$. This is shown in Fig. 11. Except for the C3SO3Na surface, no aragonite is found when the crystallization is carried out at this temperature.

SE microscopy of the SAM surfaces after crystallization at $22 \pm 3\,^{\circ}C$

Non-polar surfaces; effect of chain length. We now use the quantification of the compositions presented earlier as a rough guide to the different surfaces and attempt to examine the crystallization process more microscopically. Comparing the effects of chain length for the two least polar surfaces, C11H and C16H on which predominantly calcite and equal amounts

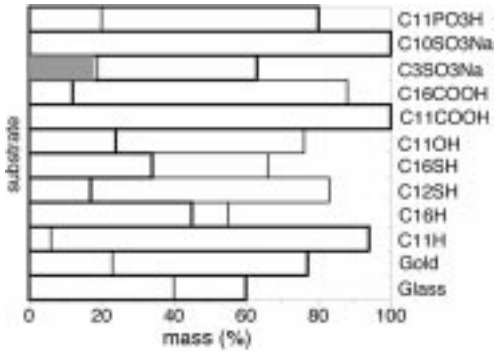

Fig. 11 Histogram of weight fractions of the $CaCO_3$ polymorphs obtained from Rietveld refinements of powder X-ray profiles from crystals of $CaCO_3$ grown at $22\pm3\,^{\circ}C$ on different substrates (indicated). The dark lines indicate the calcite mass fraction, the lighter lines correspond to vaterite and the shading to aragonite.

of calcite and vaterite were respectively obtained, we see from an analysis of the SE micrographs [Fig. 12(a) and (b)] that on C11H, neither the plate-like vaterite crystals nor the calcite rhombs show any strong tendency to grow along a particular axis. On the other hand, this tendency is clearly expressed in the case of the C16H surface. The vaterite crystals are clearly nucleated in the *ac* plane and grow very little along the *c* direction resulting in thin crystals that stand on edge. The calcite crystals are found to cluster, because of the low surface polarity, but we see from isolated crystals that the nucleating plane is (001) or (110), depending on whether the crystals stand on an apex or on an edge. The clean gold surface (not shown) also shows this kind of clustering, but there is no preferred nucleation plane on this surface. The different morphologies and compositions of the $CaCO_3$ crystals on the C11H and C16H surfaces are consistent with our expectation that the latter surface is better ordered in the plane of the SAM owing to the longer thiol chain length.

Polar surfaces; the effect of chain length. Comparing polar surfaces of differing chain lengths comprising SAMs of C11COOH and C16COOH both terminated by the carboxylate group, we see from the histogram (Fig. 11) that on the former calcite is obtained in pure yield and on the latter, vaterite predominates. Again the SE micrographs are revealing [Fig. 13(a) and (b)]. The former surface shows calcite crystals in all possible orientations while on the latter vaterite grows along the edge (*ac* plane nucleation) and calcite is nucleated on (001).

Polar surfaces; effect of ω-substituent. Comparing polar surfaces of the same chain length but different ω-substituents, C11COOH and the hydroxy terminated C11OH (micrograph in Fig. 14), the different phase compositions obtained (pure calcite in the former and mostly vaterite in the latter) seem to be due to a preferred *ab* plane nucleation of vaterite in the latter, yielding crystals sitting on their flat faces. Indeed, preliminary AFM studies suggest that despite the short chain

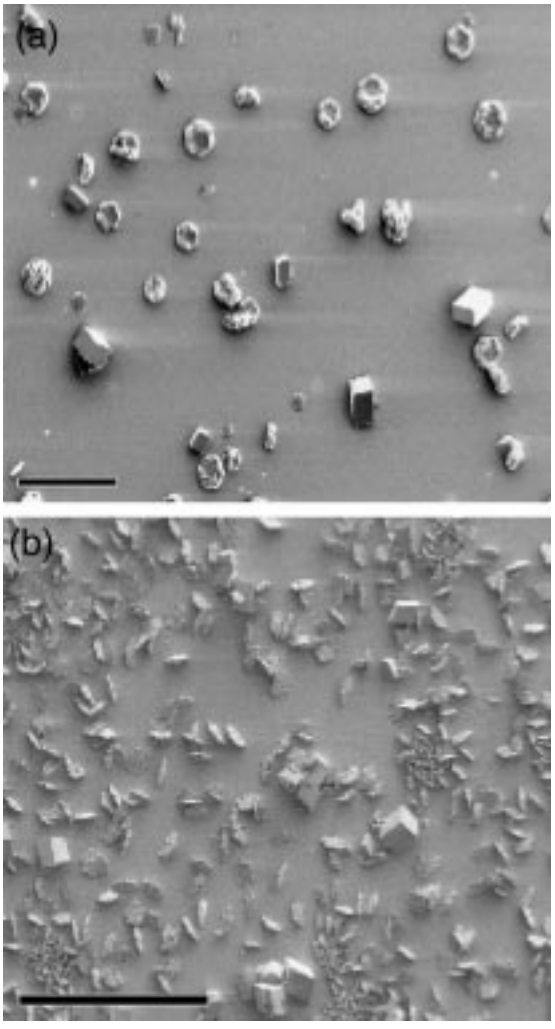

Fig. 12 SE micrographs of calcium carbonate crystals on a C11H (a) and on a C16H (b) modified gold surface at $22\pm3\,^{\circ}C$ (bars $\equiv$ 200 μm)

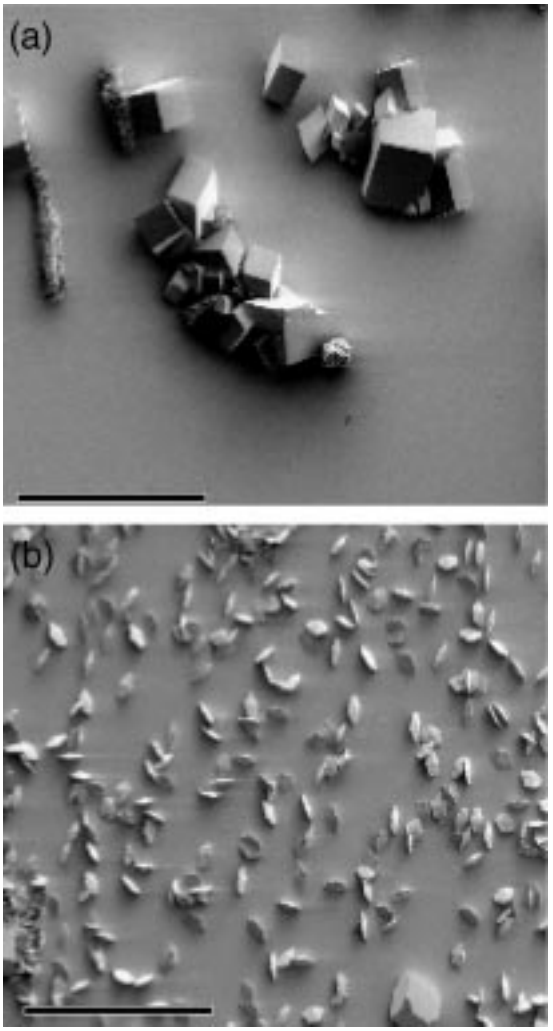

Fig. 13 SE micrographs of calcium carbonate crystals on a C11COOH (a) and on a C16COOH (b) modified gold surface at $22\pm3\,^{\circ}C$ (bars $\equiv$ 200 μm)

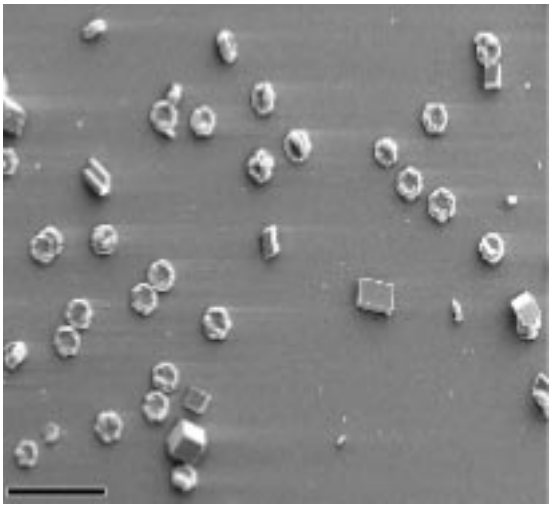

Fig. 14 SE micrograph of calcium carbonate crystals on a C11OH modified gold surface at 22 ± 3 °C (bar ≡ 200 μm)

length, the C11OH surface is ordered. Surprisingly, the calcite crystals on the C11OH surface are not nucleated on any special plane. The SAMs comprising the thiol-terminated C12SH and C16SH comprising 12 and 16 carbon atoms yield vaterite in relatively high yield (Fig. 11). The SE micrograph of the C12SH surface (Fig. 15) suggests that vaterite is again nucleated in the *ab* plane. The crystallization of calcite seems to be inhibited on this surface. Indeed, nucleation densities on surfaces with the thiol termination are small. The problem could be one of poorly formed surfaces, since dithiols tend to spontaneously form multilayers through disulfide bridges.

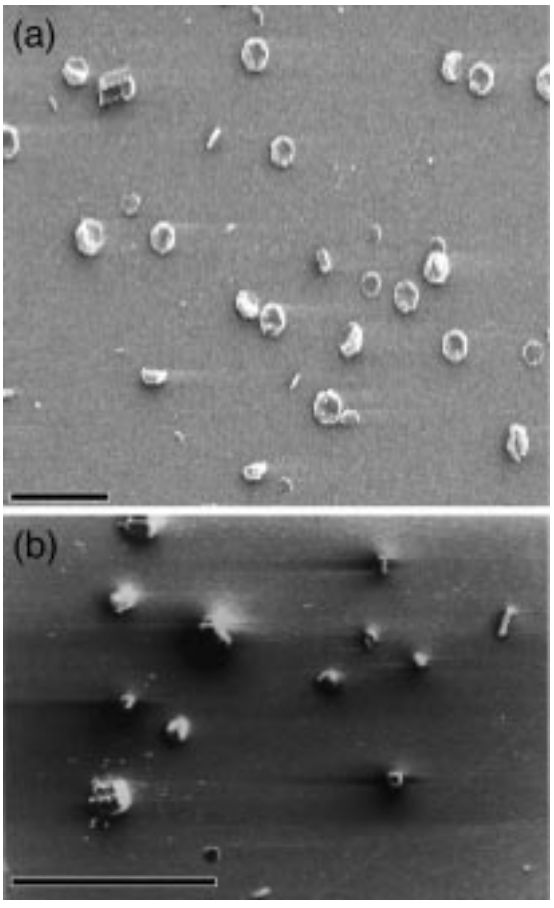

Fig. 15 SE micrographs of calcium carbonate crystals on a C12SH (a) and on a C16SH (b) modified gold surface at 22 ± 3 °C (bars ≡ 200 μm)

Crystallization at 45 ± 2 °C

The calcite–aragonite phase diagram suggests that aragonite is the stable modification above pressures of 0.4 GPa at 100 °C.[28] The stabilization of aragonite at ambient pressures would require either templating of some sort (*i.e.* nucleating aragonite preferentially over calcite) and/or the use of kinetic factors such as the degree of $CaCO_3$ supersaturation. On performing the crystallization at 45 ± 2 °C, the thermodynamics of the crystallization cannot be greatly affected, but the $(NH_4)_2CO_3$ is decomposed much more rapidly leading to greater $CaCO_3$ supersaturation in the crystallization chamber. Changing only the temperature and holding all other parameters the same, the phase compositions on the different surfaces are considerably changed. This is also known from $CaCO_3$ precipitations carried out by mixing solutions of calcium nitrate and sodium carbonate at different temperatures.[29] Temperatures higher than 40 °C yield the aragonite modification in addition to calcite and vaterite, and above 50 °C, pure aragonite may be obtained.

Fig. 16 shows typical experimental and fitted XRD profiles of $CaCO_3$ crystals collected from a C11H SAM surface after crystallization at 45 ± 2 °C. Apart from calcite, aragonite peaks now appear prominently. Again the Rietveld refined XRD scale factors have been used to calculate the mass fractions of the different phases of $CaCO_3$ for crystals obtained from growth on the different surfaces at 45 ± 2 °C and these histograms are shown in Fig. 17.

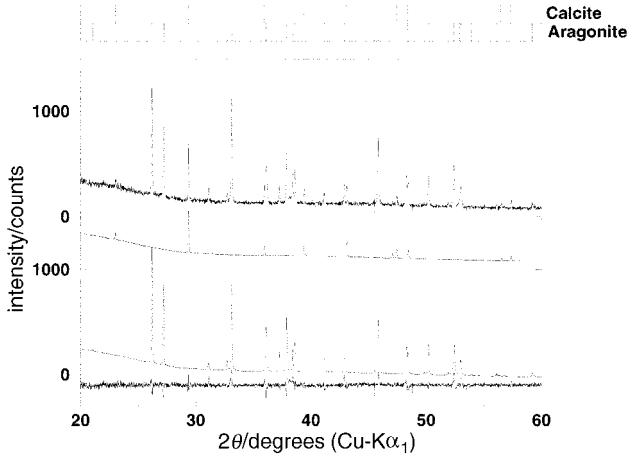

Fig. 16 Powder X-ray diffraction patterns of $CaCO_3$ crystals obtained from a C11H surface at 45 ± 2 °C. X-Ray data, Rietveld fit for the calcite and aragonite contributions and difference profiles are shown as are reflection markers. The different traces have been offset for clarity.

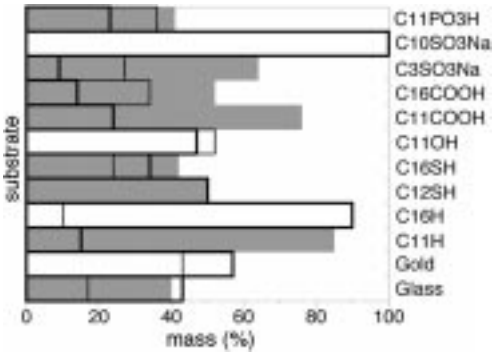

Fig. 17 Histogram of weight fractions of the $CaCO_3$ polymorphs obtained from Rietveld refinements of powder X-ray profiles from crystals of $CaCO_3$ grown at 45 ± 2 °C on different substrates (indicated). The dark lines indicate the calcite mass fraction, the lighter lines correspond to vaterite and the shading to aragonite.

Reference surfaces; glass and gold. The glass surface serves as a reference. Except for the SAM built up with C11COOH which yields *ca.* 75% aragonite and C11H which yields 85% aragonite, the other surfaces that yield aragonite (glass, C12SH, C16SH, C16COOH, C3SO3Na, C11PO3H) do so to approximately the same extent, fluctuating about a mean of *ca.* 45%. What is interesting is that certain surfaces yield no aragonite, clearly implicating the role of templating through structure and/or surface polarity. SEM of the gold surface (Fig. 18) shows calcite and vaterite crystals with no discernible orientation. No aragonite needles are seen in keeping with the XRD profile. On the glass surface, fluffy aragonite needles can be observed. There is a total absence of any preferred crystallite orientation. This last image thus corresponds to kinetically stabilized aragonite of the sort that one might obtain using the methods in ref. 23.

Effect of thiol chain length. Considering the effect of thiol chain length for two non-polar surfaces, C11H [Fig. 19(a) and (b)] and C16H [Fig. 19(c)] SE micrographs of the former show only clustered (owing to the extremely low surface energy) calcite rhombs and some vaterite (not seen in the micrograph), while the latter shows aragonite needles amidst calcite rhombs. The aragonite needles on the C11H surface also tend to cluster and are better formed than those on the glass surface. Many crystals seem to emerge out of a common nucleus which is in turn tightly bound to the surface as seen from a higher magnification image of a cluster of aragonite needles on the C11H surface. The morphology of the needles clearly comes through, the needle axis is [001]. We are not in a position to identify the nucleating plane since the fanning of the secondary needles masks the boundary between the aragonite and the templating subphase. The SE micrographs of the crystals formed on the C16COOH surface surface are of interest since vaterite forms on this surface along with aragonite and the calcite content is low. Unlike at 22 ± 3 °C, the vaterite crystals do not stand on edge but prefer to sit flat. Their habits are also rather ill formed.

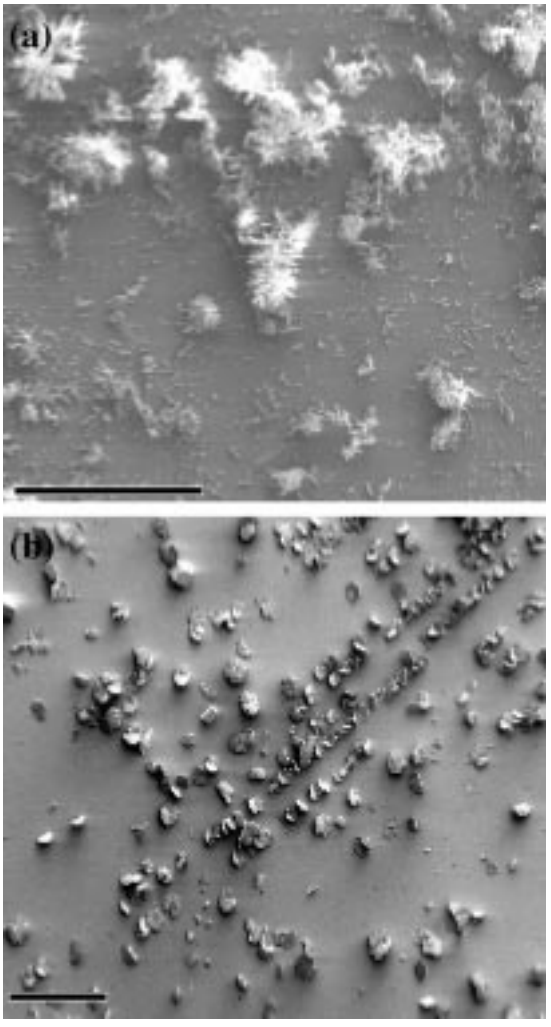

Fig. 18 SE micrographs of calcium carbonate crystals on a clean glass (a) and on a clean gold (b) surface at 45 ± 2 °C (bars $\equiv$ 200 μm)

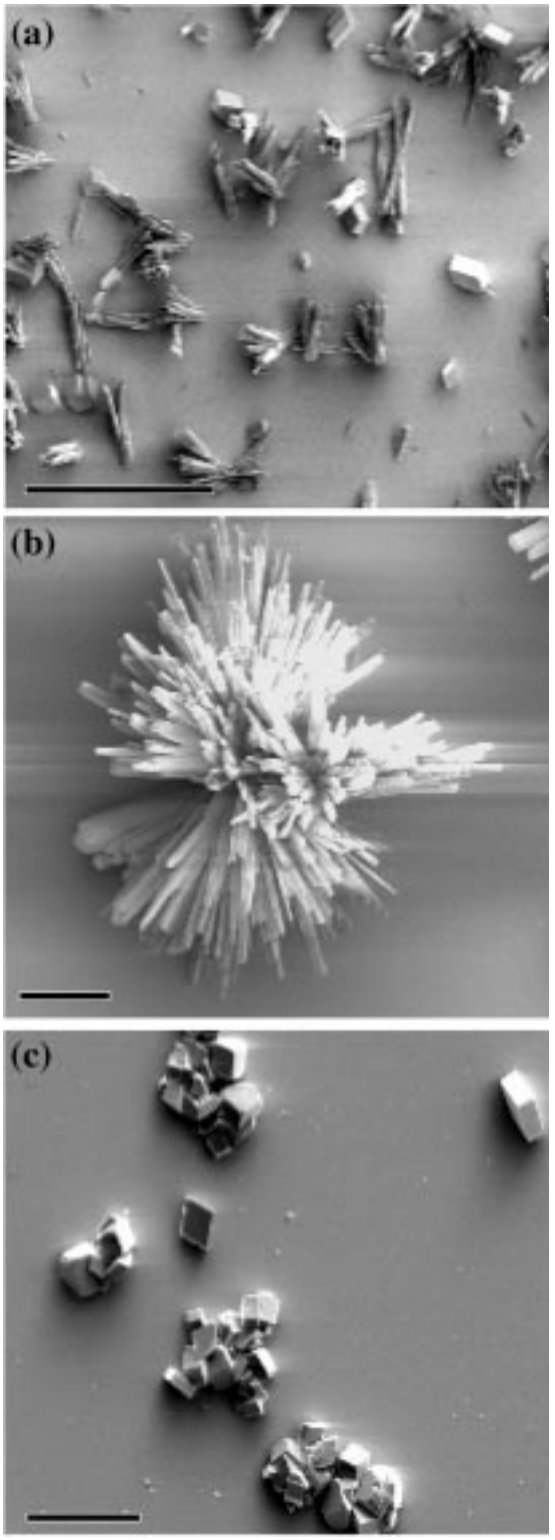

Fig. 19 SE micrographs of calcium carbonate crystals on a C11H [(a) low magnification, (b) higher magnification] and on a (c) C16H modified gold surface at 45 ± 2 °C. (a) bar $\equiv$ 200 μm; (b) bar $\equiv$ 20 μm; (c) bar $\equiv$ 50 μm.

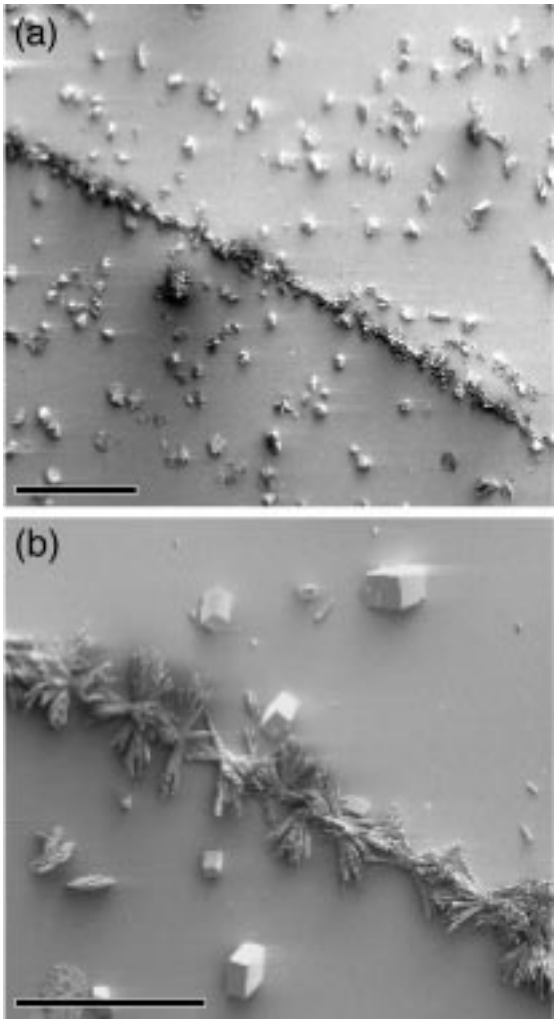

Fig. 20 SE micrographs of calcium carbonate crystals on a C16COOH modified gold surface at $45 \pm 2\,^{\circ}C$. (a) low magnification bar $\equiv 500\,\mu m$; (b) high magnification bar $\equiv 200\,\mu m$.

Low calcite content on the C16COOH surface (Fig. 20) is also seen after crystallization at $22 \pm 3\,^{\circ}C$. Another portion of this surface displays a row of clusters of aragonite needles which seem to have nucleated along a line. We assume that this line forms at the ledge of a terrace on the gold surface. The nature of the growth suggests that aragonite crystals might prefer to nucleate on rough surfaces, at ledges and crevices. We have suspected this from the comparison of the two non-polar surfaces, C16H which is highly ordered in the plane and forms no aragonite, as opposed to C11H which, having a short chain, is not expected to be well ordered in the plane of the SAM and is seen to yield a lot of aragonite. This might or might not have something to do with the fact that ordered thiols usually are hexagonally close packed on the SAM surface and thus stabilize the calcite or vaterite modifications (both with a threefold symmetry axis in the structure) but not the orthorhombic aragonite. Considering that aragonite is the high-pressure modification, another explanation can be proffered for its stabilization on rough rather than ordered surfaces. When crystallization commences in a crevice on the surface, the walls of the crevice could force, in a local manner, the growing crystal to adopt the high density modification.

The micrograph in Fig. 21 shows the sulfonate terminated C10SO3Na surface which yields pure calcite at $45 \pm 2\,^{\circ}C$. The morphology of the crystals does not suggest a preferred nucleation plane, in keeping with our expectation that this short chain (10 carbon atoms) does not form crystalline SAMs.

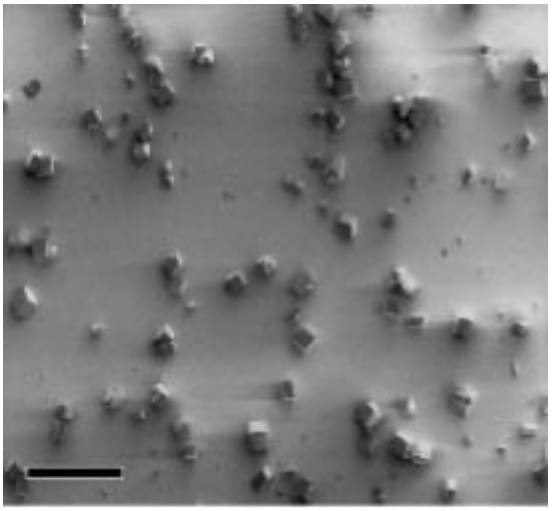

Fig. 21 SE micrograph of calcium carbonate crystals on a C10SO3Na modified gold surface at $45 \pm 2\,^{\circ}C$ (bar $\equiv 200\,\mu m$)

The absence of aragonite on this surface thus implies inhibition rather than a strong preference for calcite.

Discussion

A quantitative comparison of the ability of different SAM surfaces to template the nucleation of the three different modifications of calcium carbonate has been attempted. This has been made possible by the use of Rietveld refinement for extracting scale factors from powder X-ray profiles, complementing the more usual study by scanning electron microscopy of the habits and morphology of individual crystals.

We can compare the results in terms of phase compositions and morphologies of the calcite crystals obtained in the present study with the extensive work by Mann and co-workers[3,9,30–34] on crystallization under Langmuir monolayers. Under Langmuir monolayers of long chain carboxylates (18 carbon atoms), depending on the concentration of Ca^{2+} in solution, either calcite or vaterite are obtained.[30] On carboxylate terminated thiols at $22\,^{\circ}C$, the principal phase observed by us is calcite on C11COOH and mostly vaterite with a little calcite on C16COOH. On the sulfonate surface, we obtain calcite rich compositions, as in ref. 30. The phosphonate surface yields vaterite for Mann and co-workers whereas in our case we obtain mostly calcite. The hydroxy terminated C11OH surface yields a mixture of calcite and vaterite with inhibited growth. This is also the result of ref. 30 for hydroxy terminated monolayers. The morphologies of the calcite[30] and the vaterite[31] crystals are also largely in correspondence with those obtained by Mann and co-workers displaying rhombs for calcite and hexagonal flowerettes for vaterite. The morphology of the vaterite crystals obtained by us is distinct from the oblate, hexagonal spheroids obtained in bulk by Dupont *et al.*[35] in that in the present case they are thin and flat. Crystals of aragonite have been obtained by Mann and co-workers at room temperature under Langmuir monolayers either through the use of additives[32,33] or in a special case under a complex Langmuir monolayer[34] where there is epitaxy between orthorhombic aragonite and the monolayer. The morphologies are again similar to some of those obtained in the present study.

Conclusions

Amongst the general conclusions that can be drawn are: (i) making comparisons of the ability of clean and thiol modified gold surfaces as substrates for the crystallization of calcium carbonate, there is clear evidence for the templating effects of

the (monolayer) organic phase. The results for crystal growth at 22 °C largely match those obtained by Mann and co-workers[3,9,30–34] who use Langmuir monolayers at the air/water interface as templates.

(ii) A surprising result is that templating of calcite and vaterite takes place even on an inert surface such as C16H coated gold, with the crystals displaying marked orientations and well defined habits. The clustering of the calcite crystals and the low nucleation densities however bears witness to the inertness of the surface.

(iii) Calcite prefers to grow with large {104} faces. This means that on surfaces where no nucleation is seen the calcite rhombs are usually flat on their {104} faces. In cases of templated growth, the nucleating plane is seen to be calcite (001) which has a threefold symmetry axis and epitaxy with ordered SAMs is possible.

(iv) For crystals of vaterite, the low energy surface is {001}. (001) is also the plane with sixfold symmetry, allowing a simple epitaxial relation with the organic subphase. When crystals are sitting flat on their {001} faces, it is difficult to establish templating. However, the fact that vaterite crystals are not often seen on SAMs of short chain length thiols suggests that templating is important. On certain surfaces, vaterite grows in quantity with nucleation on (010). This is an unusual result.

(v) On SAMs built up of thiols of a given chain length, the ω-headgroup can drastically influence nucleation. Certain head groups seem to inhibit $CaCO_3$ crystallization.

(vi) Aragonite can be kinetically stabilized by elevating the temperature at which crystallization is performed to 45 °C. The effect of temperature is probably to increase the rate at which the ammonium carbonate (the source of CO_2) is decomposed, thereby resulting in a greater degree of supersaturation. However, the need for specific nuclei for aragonite crystallization even at 45 °C is observed from the absence of aragonite on certain surfaces.

(vii) On surfaces that we know are unlikely to be ordered in the plane of the SAM such as that made with the short chain length thiol C11H, we find large amounts of aragonite. As we have pointed out earlier, aragonite crystallizes in an orthorhombic space group (*Pmcn*) and has no threefold symmetry axis. There is thus no strong possibility for aragonite to grow epitaxially on the (usual) ordered SAM surface.

(viii) The needles of aragonite are seen to be clustered. The SE micrographs also show that often the majority of the aragonite needles are nucleated in a secondary manner. From this study, the nature of the primary nuclei and of the nucleating faces for aragonite cannot be unambiguously established. The absence of aragonite on certain surfaces where calcite and vaterite are present suggests that secondary nucleation of aragonite crystals by crystals of the other modifications is not a sufficient condition.

(ix) Both for crystallizations performed at 22 and at 45 °C, the order of crystalline perfection as obtained from X-ray linewidths and crystallite sizes in the SE micrographs is calcite > aragonite > vaterite. This is in keeping with the order of phase stability under ambient conditions.

References

1 A. Lowenstam and S. Weiner, *On Biomineralization*, Oxford University Press, New York, 1989.
2 *Biomineralization*, ed. S. Mann, J. Webb and R. J. P. Williams, VCH, Weinheim, 1989.
3 B. R. Heywood and S. Mann, *Adv. Mater*., 1994, **6**, 9.
4 S. Busch and R. Kniep, *Angew. Chem*., 1996, **108**, 2787.
5 B. C. Bunker, P. C. Rieke, B. J. Tarasevich, A. A. Campbell, G. E. Fryxell, G. L. Graff, L. Song, J. Liu, J. W. Virden and G. L. McVay, *Science*, 1994, **264**, 48.
6 C. D. Bain, E. B. Troughton, Y. T. Tao, J. Evall, G. M. Whitesides and R. G. Nuzzo, *J. Am. Chem. Soc*., 1989, **111**, 321.
7 P. E. Laibinis, G. M. Whitesides, D. L. Allara, Y. T. Tao, A. N. Parikh and R. G. Nuzzo, *J. Am. Chem. Soc*., 1991, **113**, 7152; A. Ulman, *Chem. Rev*., 1996, **96**, 1533.
8 D. D. Archibald, S. B. Quadri and B. P. Gaber, *Langmuir*, 1996, **12**, 538.
9 S. Mann, *J. Mater. Chem*., 1995, **5**, 935.
10 L. Leiserowitz, D. Jacquemain, S. G. Wolf, F. Leveiller, M. Deutsch, K. Kjaer, J. Als-Nielsen and M. Lahav, *Angew. Chem*., 1992, **104**, 134.
11 S. Weiner and L. Addadi, *J. Mater. Chem*., 1997, **7**, 689.
12 S. Albeck, S. Weiner and L. Addadi, *Chem. Eur. J*., 1996, **2**, 278.
13 A. Berman, L. Addadi and S. Weiner, *Nature* (*London*), 1988, **331**, 546.
14 J. Küther and W. Tremel, *Chem. Commun*., 1997, 2029.
15 H. Wolf, PhD thesis, Universität Mainz, 1995.
16 T. M. Putvinski, M. L. Schilling, H. E. Katz, C. E. D. Chidsey, A. M. Mujsce and A. B. Emerson, *Langmuir*, 1990, **6**, 1567.
17 J. Spinke, M. Liley, F. J. Schmitt, H. J. Guder, L. Angermaier and W. Knoll, *J. Chem. Phys*., 1993, **99**, 7012.
18 F. C. Meldrum, J. Flath and W. Knoll, *Langmuir*, 1997,**13**, 2033.
19 M. Bohm, CRYSDRAW.
20 R. Wartchow, *Z. Kristallogr*., 1989, **186**, 300.
21 S. R. Kamhi, *Acta Crystallogr*., 1963, **16**, 770.
22 J. P. R. de Villiers, *Am. Mineral*., 1971, **56**, 758.
23 L. H. Dubois and R. G. Nuzzo, *Annu. Rev. Phys. Chem*., 1992, **43**, 437.
24 H. M. Rietveld, *J. Appl. Crystallogr*., 1969, **2**, 65
25 J. F. Berar and P. Garnier in *Accuracy in Powder Diffraction*, *Proc. II. Intl. Conf. Gaithersburg*, 1992; *NIST Special Publ*., 1992, **846**, 212.
26 J. Rodriguez-Carvajal, *Manual of the FullProf Rietveld program; Collected Abstracts of IUCr Satellite Meeting on Powder Diffraction*, Toulouse, France, 1990, p. 127.
27 G. W. Brindley, *Philos. Mag*., 1945, **36,** 347.
28 B. R. Hacker, S. H. Kirby and S. R. Bohlen, *Science*, 1992, **258**, 110.
29 J. L. Wray and F. Daniels, *J. Am. Chem. Soc*., 1957, **79**, 2031.
30 S. Mann, F. C.Meldrum, B. R. Heywood, D. D. Archibald, J. M. Didymus and V. J. Wade, *MRS Bull*., 1992, 32.
31 S. Mann, B. R. Heywood, S. Rajam, J. B. A. Walker, R. J. Davey and J. P. Birchall, *Adv. Mater*., 1990, **2**, 257.
32 S. Mann and B. R. Heywood, *Chem. Mater*., 1994, **6**, 311.
33 S. D. Sims, J. M. Didymus and S. Mann, *J. Chem. Soc., Chem. Commun*., 1995, 1031.
34 A. L. Litvin, S. Valiyaveettil, D. L. Kaplan and S. Mann, *Adv. Mater*., 1997, **9**, 124.
35 L. Dupont, F. Portemer and M. Figlarz, *J. Mater. Chem*., 1997, **5**, 797.

Paper 7/05859D; *Received* 11*th August*, 1997